Title: Genomic evidence for West Antarctic Ice Sheet collapse during the Last Interglacial Period

Authors: Sally C. Y. Lau[1,2*], Nerida G. Wilson[3,4,5], Nicholas R. Golledge[6], Tim R. Naish[6], Phillip C. Watts[7], Catarina N. S. Silva[1,8], Ira R. Cooke[9], A. Louise Allcock[10], Felix C. Mark[11], Katrin Linse[12], Jan M. Strugnell[1,2]

Affiliations:

[1]Centre for Sustainable Tropical Fisheries and Aquaculture and College of Science and Engineering, James Cook University; Townsville, Qld, Australia

[2]Securing Antarctica's Environmental Future, James Cook University, Townsville, Qld, Australia

[3]Collections & Research, Western Australian Museum; Welshpool, WA, Australia

[4]School of Biological Sciences, University of Western Australia; Perth, WA, Australia

[5]Securing Antarctica's Environmental Future, Western Australian Museum; Welshpool, WA, Australia

[6]Antarctic Research Centre, Victoria University of Wellington; Wellington, New Zealand

[7]Department of Biological and Environmental Science, University of Jyväskylä; Jyväskylä, Finland

[8]Nature Research Centre; Vilnius, Lithuania

[9]Centre for Tropical Bioinformatics and Molecular Biology, James Cook University; Townsville, Qld, Australia

[10]School of Natural Sciences and Ryan Institute, National University of Ireland Galway; Galway, Ireland

[11]Alfred Wegener Institute, Helmholtz Centre for Polar and Marine Research; Bremerhaven, Germany

[12]British Antarctic Survey; Cambridge, United Kingdom

*Corresponding author. Email: cheukying.lau@jcu.edu.au

Abstract:

The marine-based West Antarctic Ice Sheet (WAIS) is considered vulnerable to collapse under future climate trajectories and may even lie within the mitigated warming scenarios of 1.5–2 ºC of the United Nations Paris Agreement. Knowledge of ice loss during similarly warm past climates, including the Last Interglacial period, when global sea levels were 5–10 m higher than today, and global average temperatures of 0.5–1.5 ºC warmer, could resolve this uncertainty. Here we show, using a panel of genome-wide, single nucleotide polymorphisms of a circum-Antarctic octopus, persistent, historic signals of gene flow only possible with complete WAIS collapse. Our results provide the first empirical evidence that the tipping point of WAIS loss could be reached even under stringent climate mitigation scenarios.

One-Sentence Summary:

Historical gene flow in marine animals indicate the West Antarctic ice sheet collapsed during the Last Interglacial period.

Climate change continues to cause unprecedented warming to the Earth system (*1*). The consequences of warming are leading to rapid changes in Antarctica, including Antarctic Ice Sheet mass loss, with global impacts (*1*). A major uncertainty in global mean sea level (GMSL) rise projections lies in the stability of the West Antarctic Ice Sheet (WAIS) (*2*). The marine-based WAIS has lost 159 ± 8 gigatons of ice mass per year between 1979–2017 (*3*), and will continue to be a major contributor to GMSL rise under all CO_2 emission scenarios (*4*). It is unclear whether the WAIS is vulnerable to rapid ice loss or even full collapse, because of a poor understanding of future changes and processes that influence ice sheet dynamics (*2*). A complete WAIS collapse could raise global sea level by ~3.3–5 m (*5*, *6*), with direct consequences that include human displacement and global loss of ecosystems in coastal areas (*1*).

It is well understood from geological reconstructions that there were interglacial peaks (i.e. super-interglacials) in periods of the Pleistocene that experienced warmer temperatures (+~0.5–5.0 ºC) and higher GMSL (+~5–20 m) than present (*4*). These super-interglacials include Marine Isotope Stages (MIS) 31, 11 and 5e, which occurred at approximately ~1.08–1.05 Ma, ~424–395 ka and ~129–116 ka, respectively (*4*). During MIS 31, the average surface sea temperature (SST) was +5 ± 1.2 ºC with GMSL ~20 m higher than present (*7*). During MIS 11, global mean surface temperature (GMST) was 0.5 ± 1.6ºC with GMSL 6–13 m higher than present, and similarly, during MIS 5e (the Last Interglacial period), GMST was +0.5–1.5ºC with GMSL 5–10 m higher than present (*4*). To date, there is no empirical evidence to indicate if the WAIS has completely collapsed at any time in the three million years since the Pliocene (*8*). Inferring WAIS configurations during late Pleistocene super-interglacial periods could therefore inform the sensitivity of Antarctic ice-sheet response to climate change. So far, analyses of ice proximal marine drill core records show evidence of WAIS retreat during the late Pleistocene interglacials,

but the exact timing (*9*) and extent (*10*, *11*) of any WAIS collapse remain ambiguous. Existing ice sheet models have yielded conflicting WAIS reconstructions during these periods, ranging from no collapse (*12*), to partial (*13*) or full collapse (*14*, *15*). Knowledge about how the WAIS was configured during super-interglacials in the geological past is urgently needed to constrain future sea level rise projections (*2*). Novel approaches, such as population genomics, can serve as empirical proxies of past changes to the Antarctic ice sheets, detected via signals of historic gene flow among currently separated populations of marine organisms (*16*).

A complete past collapse of the WAIS would have opened the trans-West Antarctic seaways linking the present-day Weddell Sea (WS), Amundsen Sea (AS) and Ross Sea (RS) (*16*). Such seaways would have allowed marine benthic organisms to occupy and disperse across the opened straits, thus leaving genetic signatures of this past connectivity in the genomes of their descendent, extant populations (*16*) (hereafter seaway populations). As the WAIS reformed, these organisms would be isolated again within the WS, AS and RS basins, with any subsequent connectivity only possible around the continental margin. Although there is some support for existence of trans-Antarctic seaways based on species assemblage data at macro-evolutionary scales (*17–20*) or low-resolution genetic data (*21–24*), all these studies lack power and/or spatial coverage to distinguish between past dispersal via trans-West Antarctic seaways or from contemporary circumpolar ocean currents. Importantly, these previous studies cannot be used for accurate demographic modelling to identify the likely timing of any collapse in the WAIS.

Collection of benthic species from the Southern Ocean is logistically challenging and regions such as AS and East Antarctica (EA) are difficult to access. Existing samples are typically characterised by DNA degradation due to long term storage in collections at room temperature.

Here, we used a target capture approach that sequenced genome-wide, single nucleotide polymorphism (SNP) data in the circum-Antarctic benthic octopus, *Pareledone turqueti*, incorporating rare samples from AS and EA, collected over 32 years. Our approach enabled a comprehensive sampling strategy to robustly date and test for the presence of past trans-West Antarctic seaways using biological data as proxies.

We sequenced genome-wide SNPs derived from double-digest restriction site-associated DNA (ddRAD) (*25*) loci from 96 *P. turqueti* individuals collected from around the Southern Ocean (Fig. 1A). The dataset presents a circum-Antarctic overview of the species genetic patterns, which record the contemporary connectivity driven by oceanic currents, mainly the Antarctic circumpolar current (ACC; clockwise) and the Antarctic Slope Current (ASC; counter-clockwise) (Fig. 1A, B), as well as any historical connectivity that would be associated with past trans-West Antarctic seaways. We used a reduced single-nucleotide polymorphisms (SNPs) dataset (one SNP per locus) to analyse population structure, which included 5,188 unlinked SNPs. The population genomic variation of *P. turqueti* is characterised by geographically-structured populations across the Southern Ocean (Fig. 1C, fig. S1-S2), as expected for a marine species with benthic crawling hatchlings. This makes it an appropriate species to test for the presence of trans-West Antarctic seaways. Long-distance connectivity linking East and West Antarctica, across the Antarctic continental shelf and Antarctic islands, is detected, likely indicating dispersal that reflects contemporary circumpolar currents, as found in other Southern Ocean benthic taxa (*26*). However, admixture is also observed between individuals from RS and AS with some individuals from WS (Fig. 1C, fig. S1), indicating a potential signature of trans-West Antarctic seaways.

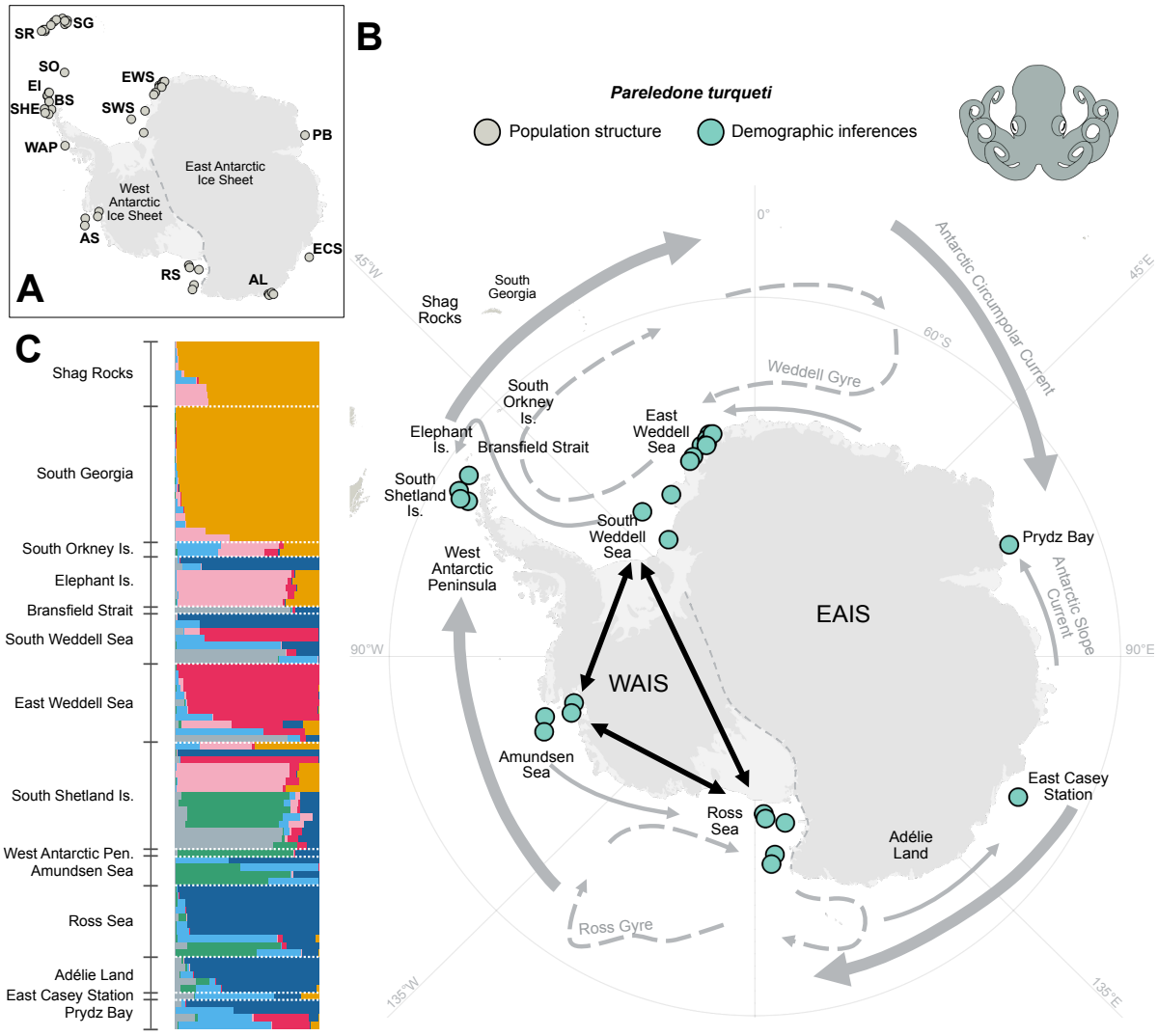

Fig. 1 Sample locations of *Pareledone turqueti* with *Structure* analyses. (**A**) Samples used for analyses of population structure. Abbreviations: Shag Rocks, SR; South Georgia, SG; South Orkney Is., SOI; Elephant Is., EI; Bransfield Strait, BS; South Shetland Is., SHE; West Antarctic Peninsula, WAP; South- and East- Weddell Sea, S-, E-WS; Amundsen Sea, AS; Ross Sea, RS; Adélie Land, AL; East Casey Station, ECS; Prydz Bay, PB; West Antarctic Ice Sheet, WAIS; East Antarctic Ice Sheet, EAIS. (**B**) Samples used for admixture analyses and demographic modelling (collectively demographic inferences) to test for the existence of trans-West Antarctic seaways. Map include the directionalities of the major contemporary circumpolar currents and regional currents in the Southern Ocean. Black arrows indicate connectivity pathways through trans-West Antarctic seaways that would result from WAIS collapse. Direct connectivity between WS-AS or AS-RS would indicate partial WAIS collapse, and direct connectivity between WS-AS-RS or WS-RS would indicate complete WAIS collapse. (**C**) Clustering analysis using *Structure* inferred $K = 7$ for *P. turqueti*. Each horizontal bar represents an individual sample, bars are grouped by geographical locations, colours within each bar correspond to the proportion of each genetic cluster in the individual.

130 Focusing on populations most informative of whether WAIS collapsed in the past, we first
131 examined whether there was distinct admixture between WS-AS-RS with respect to South
132 Shetland Islands (SHE) and East Antarctica (EA; including Prydz Bay and East Casey Station)
133 samples using 120,857 linked sites (i.e. all SNPs retained across loci) (Fig. 1B). SHE and EA are
134 known to be influenced by both the ACC and ASC (*27*), but are peripheral to the putative
135 historical trans-West Antarctic connectivity; thus these are ideal locations that can separate
136 patterns of present-day connectivity around the WAIS and East Antarctic Ice Sheet (EAIS) from
137 persistent, historical signals of gene flow.
138
139 We examined allele frequency correlations across WS, AS and RS with respect to SHE and EA.
140 The *D*-statistic (*28*) explores the patterns of alleles sharing across four populations to test for
141 evidence of admixture between populations of interest. The outgroup-f_3-statistic (*29*) explores
142 the amount of derived allele frequency that is shared between pairs of populations relative to an
143 outgroup population. The presence of admixture linked to trans-West Antarctic connectivity
144 would result in high f_3 values, and evidence of excess allele sharing (D>0), between WS-AS-RS.
145 In *P. turqueti*, the highest f_3 values are detected between AS–RS, followed by RS–EA and RS–
146 WS (Fig. 2A); indicating recent common ancestry across seaway populations, as well as between
147 RS and EA populations that are adjacent to each other. When SHE is treated as the sister lineage
148 to AS/RS and WS (*D*(AS/RS, SHE, WS, outgroup)), there is excess allele sharing between
149 AS/RS and WS (Fig. 2B). When EA is treated as sister lineage to AS/RS and WS (*D*(AS/RA,
150 EA, WS, outgroup)), excess allele sharing is also observed between AS/RS and WS (Fig. 2B).
151 These results confirm that, in *P. turqueti*, there are unexpected, and significant, allele frequency
152 correlations among AS-RS-WS, despite also considering the locations situated between them
153 around the WAIS (SHE) and EAIS (EA). Such observed admixture patterns are congruent with

historical seaway connectivity in a species that is characterised by geographically-structured populations.

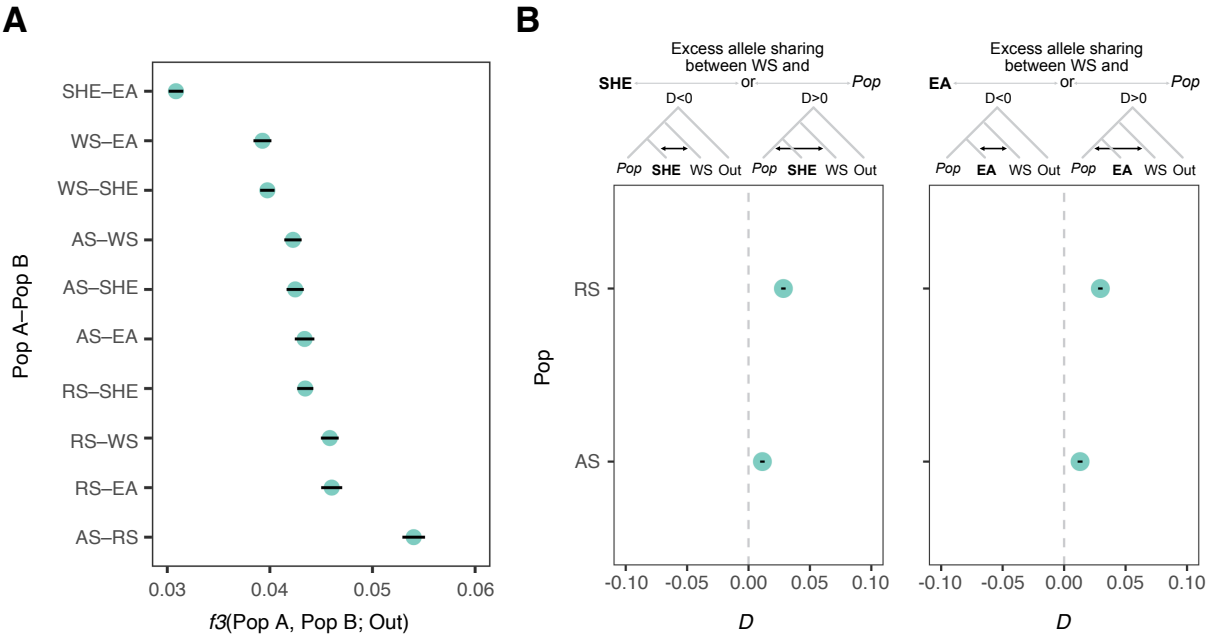

Fig. 2 Evidence of distinct allele frequency correlations between Amundsen Sea, Weddell Sea and Ross Sea, as well as contemporary gene flow in *Pareledone turqueti*. Error bars (black horizonal lines) = standard errors, filled circles = significant (Z-score values > 3 or < -3), Out = outgroup population, which includes Shag Rocks and South Georgia (samples combined). Abbreviations: Weddell Sea (WS), South Shetland Islands (SHE), Amundsen Sea (AS), Ross Sea (RS), East Antarctica (EA). (**A**) Outgroup-f_3-statistics between pairs of populations. As f_3 value increases, more derived allele frequency is shared between the pairs of population. (**B**) *D*-statistic (in the form of BABA-ABBA) examines patterns of alleles sharing across four populations, and indicates whether there is excess allele sharing between distinct populations. Left panel: *D*-statistic is presented in the form of *D*(Pop, SHE, WS, Out), which examines whether there is excess allele sharing between SHE and WS (*D*<0; ABBA) or Pop and WS (*D*>0; BABA). Right panel: *D*-statistic is presented in the form of *D*(Pop, EA, WS, Out), which examines whether there is excess allele sharing between EA and WS (*D*<0; ABBA) or Pop and WS (*D*>0; BABA).

172 A site-frequency-spectrum (SFS)-based, coalescent demographic modelling framework
173 (*fastsimcoal* (*30*)) was used to test the hypothesis of whether historical trans-Antarctic seaways
174 existed, with populations subsequently influenced by contemporary circumpolar gene flow. For
175 demographic modelling, we included samples from WS, AS, RS and EA with 189,248 linkage
176 disequilibrium (LD)-pruned sites across loci in *P. turqueti*. We employed a hierarchical approach
177 to test for WAIS collapse scenarios while incorporating modern circumpolar gene flow in the
178 models (fig. S3-S4). Step 1 compared contrasting scenarios of past WAIS configurations with
179 circumpolar gene flow following the directionality of the ACC (clockwise). The models
180 incorporated WS, EA, RS and AS experiencing continuous circumpolar gene flow since
181 population divergence. Under these scenarios, after population divergence, WS, AS, RS
182 experienced no, partial, or complete connectivity, followed by modern ACC gene flow linking
183 between WS, EA, RS and AS. In, step 2, model complexity was increased, with circumpolar
184 gene flow following both directionalities of the ACC and ASC (counter-clockwise) for all
185 scenarios.
186
187 The observed SFSs were statistically best explained by the scenario of a complete historical
188 WAIS collapse (Fig. 3A), followed by modern circumpolar gene flow linked to ACC and ASC.
189 The ancestral lineage of WS, AS, RS and EA populations experienced an expansion at 1.8 Mya
190 (95% confidence interval [CI] between 1.9–6.0 Mya) (Fig. 3A, table S1). Such CI range,
191 measured within one parameter that captures signals of ancestral demographic changes, likely
192 reflects noise from multiple scenarios that happened in the past. For example, based on
193 mitochondrial data (*23*), lower CI (1.9 Mya) corresponds to the previous estimated timing of the
194 diversification of the continental shelf clades, whereas the upper CI (6.0 Mya) corresponds to the
195 timing of species divergence. The signal of ancestral population growth detected in the

196 demographic model, as well as the evolutionary scenarios proposed, support demographic
197 change linked to range expansion across the Antarctic continental shelf. Then, at 70 ka (95% CI
198 between 68 and 265 ka), the best model supports WS, AS, RS and EA locations splitting into
199 four populations with direct asymmetric gene flow detected. Direct gene flow was detected from
200 RS to WS (n=3.76e^{-3} migrants per generation; 95% CI between 3.37e^{-5}–2) and WS to RS
201 (=1.58e^{-3} migrants per generation; 95% CI between 3.67e^{-6}–1); a direct historical connection was
202 detected between WS and RS. This suggests that an ancient seaway was likely once opened
203 across the WAIS, which directly linked the present day WS and RS. This could only be
204 facilitated by a complete WAIS collapse during an interglacial period, which we infer to have
205 occurred approximately between 68 and 265 ka (based on 95% CI; Fig. 3A), and which is in
206 accordance with MIS 5e, the most recent or Last Interglacial.
207
208 The time lag between the direct connectivity between RS and WS at 70 ka (value at maximum
209 likelihood) and the time of MIS 5e (129–116 ka) likely reflects the time it takes for complete
210 trans-West Antarctic migration to influence allele frequencies in a benthic direct developing
211 octopus. Finally, contemporary circumpolar gene flow began at 22 ka (95% CI between 28–196
212 ka), following the opposite directions as the ACC and ASC, which reflects how modern gene
213 flow in benthic taxa is influenced by ongoing circumpolar currents, in particular the ACC (*26*);
214 which has been stable since the LGM (20 ka) (*31*).
215

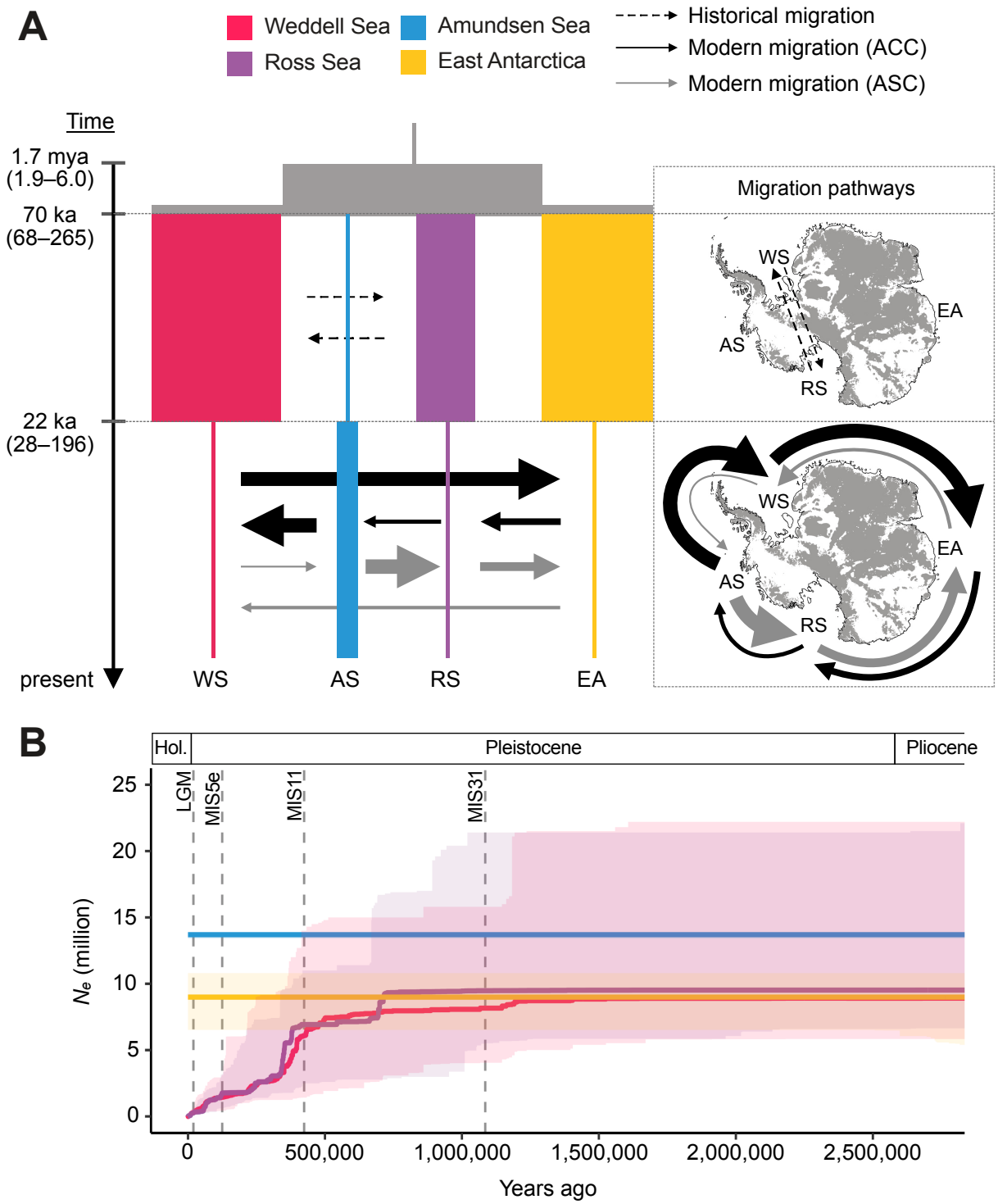

Fig. 3 The best-supported demographic model for *Pareledone turqueti* indicated a complete historical West Antarctic Ice Sheet collapse scenario at Marine Isotope Stage (MIS) 5e, supplemented by a *StairwayPlot* which indicated past changes in population size. (**A**) Maximum likelihood model for *P. turqueti* including Amundsen Sea (AS), Ross Sea (RS), Weddell Sea (WS) and East Antarctica (EA) populations, shows direct historical gene flow (70–22 ka) between WS and RS, and modern gene flow (22–0 ka) following the directionality of the Antarctic Circumpolar Current (ACC; clockwise) and Antarctic Slope Current (ASC; counter-

clockwise). Maximised parameter estimates are visualised. The associated 95% confidence intervals (CI) are in brackets and reported in Table S1. Time of the events modelled are shown on the left. The width of the bars is proportional to the effective population size of the population. Arrows indicate immigration (forward in time), with the width of the arrows proportional to the number of immigrants received (2Nm). The migration pathways, based on modelled migration directions (forward in time), are also visualised on a map of Antarctica. Map shows sub-glacial bed elevation >0 m above present-day sea level and is extracted from Bedmap2 (*32*). (**B**) *StairwayPlot* reconstruction of past changes in effective population size over time in *P. turqueti* since species divergence. Dashed vertical lines represent timing of the Last Glacial Maximum (LGM; ~20 ka), Marine Isotope Stage 5e (MIS 5e; ~125 ka), Marine Isotope Stage 11 (MIS 11; ~424 ka) and Marine Isotope Stage 31 (MIS 31; ~1.08 mya). Abbreviation: Holocene, Hol.

One of the biggest challenges of inferring demographic events in the late Pleistocene include whether the species experienced a severe bottleneck (i.e. sharp reduction in N_e) in the recent past that eroded genomic history. For example, if the WAIS had collapsed in the late Pleistocene, large areas of newly ice-free habitats (where the WAIS existed previously) would have become available for benthic fauna to disperse and colonise. During the subsequent glacial maximum, as the AIS expanded across the Antarctic continental shelf, the marine shelf habitats would likely be reduced to small, isolated pockets of *in situ* ice-free refugia (*33*). Such changes in habitat availability would likely lead to severe population bottlenecks and subsequent genetic drift (*33*). As a result, the presence of a severe recent bottleneck could lead to a loss of alleles and potentially confound parameter scaling in demographic models (*30*).

We searched for signals of population size fluctuation prior to the LGM in *P. turqueti* using *StairwayPlot* (*34*), an SFS-based model-free method. We found that the demographic changes dated by *StairwayPlot* correspond with the dating of gene flow changes by *fastsimcoal*. Throughout *P. turqueti*'s evolutionary history, pronounced demographic changes (in the form of population size decline) were detected in the RS and WS populations at ~418–335 ka, ~125–55

253 ka, and ~20–0 ka. These timings coincide with MIS 11, MIS 5e and LGM, respectively. The
254 sharp population decline detected in RS and WS around MIS 11 and MIS 5e corresponds to the
255 hypothesised scenario that N_e would experience a dramatic bottleneck had the WAIS collapsed,
256 then reformed and expanded across the Antarctic continental shelf following the end of a super-
257 interglacial. The population decline detected in RS and WS around LGM also corresponds to the
258 widely-accepted hypothesis that there would be limited *in situ* ice-free refugia on the Antarctic
259 continental shelf during this period, leading to population bottlenecks in benthic species that only
260 survived on the shelf (*33*) (i.e. the case for *P. turqueti* (*23*)). Sharp bottlenecks also represent a
261 signal of fluctuations in population size at that time interval (*34*). These patterns suggest that
262 recent super-interglacials and the LGM likely strongly influenced species demography,
263 particularly in populations associated with the signatures of WAIS collapse.
264
265 Since the demographic modelling used in this study is based on the backward-facing coalescent
266 process, the best-supported demographic model was able to characterise major demographic
267 changes during the LGM and MIS 5e (the most recent timepoints). Estimation of past changes in
268 population size indicated AS and EA populations experienced stable populations over time,
269 while *fastsimcoal* indicated population size changes; such discordances are likely due to method-
270 specific sensitivity in populations with low sample size in regions that are challenging to collect
271 biological samples (n≤5 in AS and EA). Low sample size in AS also likely reduced the power of
272 demographic models to detect historical trans-West Antarctic connectivity between AS and
273 WS/RS, despite the apparent distinct allele frequency correlations detected between them.
274 Overall, the timing of demographic events detected by independent inferences corroborates the
275 timings of major glacial-interglacial fluctuations in the late Pleistocene, as well as events dated
276 using independent markers (mitochondrial data) (*23*). Therefore, the dating of WAIS collapse

during MIS 5e as seen through the genomic data of *P. turqueti* appears to be robust and unconfounded by noise.

Our demographic modelling approach was specifically designed to test whether trans-West Antarctic seaways existed in the past that could be detected with simple contrasting models. The evolutionary history of *P. turqueti* is highly complex and populations would have experienced unique demographic changes associated with each glacial-interglacial cycle throughout the Quaternary. We utilised a target capture approach that can sequence reduced representation genomic data in samples with DNA degradation. We did not sequentially reconstruct their past changes in population size and connectivity patterns to avoid over-parameterisation in limited SNP datasets. Regardless of the overall challenge of demographic modelling for Southern Ocean species, signatures of a complete WAIS collapse, likely during the MIS 5e, were clearly detectable in *P. turqueti*.

Here we provide empirical evidence indicating the WAIS collapsed during the Last Interglacial period (MIS 5e), when global mean surface temperature was 0.5–1.5 ºC warmer than the pre-industrial. Currently, future WAIS collapse on centennial timescales is considered as a low likelihood process (*4*). In recent trajectories estimated for temperature rise, such as for the most optimistic emission scenario Shared Socio-economic Pathway (SSP) 1-1.9, the air temperature is projected to reach +1.2–1.7 ºC by 2100 (very likely range) (*4*), which is potentially within the tipping point of future WAIS collapse. Future global sea level rise projections should consider the potential feedbacks caused by collapse of the WAIS, which could lead to catastrophic GMSL rise in the range of 3.3–5 m (*5*, *6*) under relevant SSP scenarios (SSP1–5) (*35*). Accurate

predictions are necessary to ensure that better decisions are made regarding the socioeconomic, demographic, institutional, and political policies of global coastal communities.

References

1. IPCC, *Climate Change 2021: The Physical Science Basis. Contribution of Working Group I to the Sixth Assessment Report of the Intergovernmental Panel on Climate Change* (Cambridge University Press, Cambridge and New York, 2021).
2. F. Pattyn, M. Morlighem, The uncertain future of the Antarctic Ice Sheet. *Science*. **367**, 1331–1335 (2020).
3. E. Rignot *et al.*, Four decades of Antarctic Ice Sheet mass balance from 1979–2017. *Proc. Natl. Acad. Sci. U.S.A*. **115**, 1095–1103 (2019).
4. B. Fox-Kemper *et al.*, "Chapter 9: Ocean, cryosphere, and sea level change" in *Climate Change 2021: The Physical Science Basis. Contribution of Working Group I to the Sixth Assessment Report of the Intergovernmental Panel on Climate Change* (Cambridge University Press, Cambridge and New York, 2021).
5. D. G. Vaughan, West Antarctic Ice Sheet collapse – the fall and rise of a paradigm. *Clim. Change*. **91**, 65–79 (2008).
6. J. L. Bamber, R. E. M. Riva, B. L. A. Vermeersen, A. M. Lebrocq, Reassessment of the potential sea-level rise from a collapse of the West Antarctic Ice Sheet. *Science*. **324**, 901–903 (2009).
7. C. Beltran *et al.*, Southern Ocean temperature records and ice-sheet models demonstrate rapid Antarctic ice sheet retreat under low atmospheric CO2 during Marine Isotope Stage 31. *Quat. Sci. Rev.* **228**, 106069 (2020).
8. G. R. Grant *et al.*, The amplitude and origin of sea-level variability during the Pliocene epoch. *Nature*. **574**, 237–241 (2019).

9. R. P. Scherer *et al.*, Antarctic records of precession-paced insolation-driven warming during early Pleistocene Marine Isotope Stage 31. *Geophys. Res. Lett*. **35**, L03505 (2008).

10. R. McKay *et al.*, Pleistocene variability of Antarctic Ice Sheet extent in the Ross Embayment. *Quat. Sci. Rev*. **34**, 93–112 (2012).

11. T. Naish *et al.*, Obliquity-paced Pliocene West Antarctic ice sheet oscillations. *Nature*. **458**, 322–328 (2009).

12. M. D. Holloway *et al.*, Antarctic last interglacial isotope peak in response to sea ice retreat not ice-sheet collapse. *Nature Communications*. **7**, 12293 (2016).

13. N. R. Golledge *et al.*, Retreat of the Antarctic Ice Sheet During the Last Interglaciation and Implications for Future Change. *Geophys. Res. Lett*. **48**, e2021GL094513 (2021).

14. E. J. Steig *et al.*, Influence of West Antarctic Ice Sheet collapse on Antarctic surface climate. *Geophys. Res. Lett*. **42**, 4862–4868 (2015).

15. R. M. DeConto, D. Pollard, Contribution of Antarctica to past and future sea-level rise. *Nature*. **531**, 591–597 (2016).

16. J. M. Strugnell, J. B. Pedro, N. G. Wilson, Dating Antarctic ice sheet collapse: Proposing a molecular genetic approach. *Quat. Sci. Rev*. **179**, 153–157 (2018).

17. K. Linse, H. J. Griffiths, D. K. A. Barnes, A. Clarke, Biodiversity and biogeography of Antarctic and sub-Antarctic Mollusca. *Deep-Sea Res. II: Top. Stud. Oceanogr*. **53**, 985–1008 (2006).

18. D. K. A. Barnes, C. D. Hillenbrand, Faunal evidence for a late quaternary trans-Antarctic seaway. *Glob. Chang. Biol*. **16**, 3297–3303 (2010).

19. D. G. Vaughan, D. K. A. Barnes, P. T. Fretwell, R. G. Bingham, Potential seaways across West Antarctica. *Geochemistry, Geophys. Geosystems.* **12**, Q10004 (2011).

20. C. Moreau *et al.*, Is reproductive strategy a key factor in understanding the evolutionary history of Southern Ocean Asteroidea (Echinodermata)? *Ecology and Evolution*. **9**, 8465–8478 (2019).

21. C. Held, J. W. Wägele, Cryptic speciation in the giant Antarctic isopod *Glyptonotus antarcticus* (Isopoda, Valvifera, Chaetiliidae). *Sci. Mar*. **69**, 175–181 (2005).

22. K. Linse, T. Cope, A.-N. Lörz, C. Sands, Is the Scotia Sea a centre of Antarctic marine diversification? Some evidence of cryptic speciation in the circum-Antarctic bivalve *Lissarca notorcadensis* (Arcoidea: Philobryidae). *Pol. Biol*. **30**, 1059–1068 (2007).

23. J. M. Strugnell, P. C. Watts, P. J. Smith, A. L. Allcock, Persistent genetic signatures of historic climatic events in an Antarctic octopus. *Mol. Ecol*. **21**, 2775–2787 (2012).

24. G. E. Collins *et al.*, Genetic diversity of soil invertebrates corroborates timing estimates for past collapses of the West Antarctic Ice Sheet. *Proc. Natl. Acad. Sci. U.S.A*. **36**, 22293–22302 (2020).

25. B. K. Peterson, J. N. Weber, E. H. Kay, H. S. Fisher, H. E. Hoekstra, Double Digest RADseq: An Inexpensive Method for De Novo SNP Discovery and Genotyping in Model and Non-Model Species. *PLoS One*. **7**, e37135 (2012).

26. A. Riesgo, S. Taboada, C. Avila, Evolutionary patterns in Antarctic marine invertebrates: An update on molecular studies. *Mar. Genomics*. **23**, 1–13 (2015).

27. A. F. Thompson, A. L. Stewart, P. Spence, K. J. Heywood, The Antarctic Slope Current in a Changing Climate. *Rev. Geophys*. **56**, 741–770 (2018).

28. E. Y. Durand, N. Patterson, D. Reich, M. Slatkin, Testing for ancient admixture between closely related populations. *Mol. Biol. Evol*. **28**, 2239–2252 (2011).

29. M. Raghavan *et al.*, Upper Palaeolithic Siberian genome reveals dual ancestry of Native Americans. *Nature*. **505**, 87–91 (2014).

30. L. Excoffier, I. Dupanloup, E. Huerta-Sánchez, V. C. Sousa, M. Foll, Robust Demographic Inference from Genomic and SNP Data. *PLoS Genet*. **9**, e1003905 (2013).

31. I. N. McCave, S. J. Crowhurst, G. Kuhn, C.-D. Hillenbrand, M. P. Meredith, Minimal change in Antarctic Circumpolar Current flow speed between the last glacial and Holocene. *Nat. Geosci*. **7**, 113–116 (2014).

32. P. Fretwell *et al.*, Bedmap2: improved ice bed, surface and thickness datasets for Antarctica. *The Cryosphere*. **7**, 375–393 (2013).

33. A. L. Allcock, J. M. Strugnell, Southern Ocean diversity: new paradigms from molecular ecology. *Trends Ecol. Evol*. **27**, 520–528 (2012).

34. X. Liu, Y.-X. Fu, Exploring Population Size Changes Using SNP Frequency Spectra. *Nat. Genet*. **47**, 555–559 (2015).

35. M. Meinshausen *et al.*, The shared socio-economic pathway (SSP) greenhouse gas concentrations and their extensions to 2500. *Geosci. Model Dev*. **13**, 3571–3605 (2020).

36. J. M. Strugnell, A. L. Allcock, P. C. Watts, Closely related octopus species show different spatial genetic structures in response to the Antarctic seascape. *Ecol. Evol*. **7**, 8087–8099 (2017).

37. J. M. Catchen, A. Amores, P. Hohenlohe, W. Cresko, J. H. Postlethwait, Stacks: Building and Genotyping Loci De Novo From Short-Read Sequences. *G3: Genes Genomes Genet*. **1**, 171–182 (2011).

38. S. Chen, Y. Zhou, Y. Chen, J. Gu, fastp: an ultra-fast all-in-one FASTQ preprocessor. *Bioinform*. **34**, i884–i890 (2018).

39. D. E. Wood, S. L. Salzberg, Kraken: ultrafast metagenomic sequence classification using exact alignments. *Genome Biol.***15**, R46 (2014).

40. S. Andrews, FastQC: A Quality Control tool for High Throughput Sequence Data. *Babraham Institute* (2019).

41. H. Li, R. Durbin, Fast and accurate short read alignment with Burrows–Wheeler transform. *Bioinform*. **25**, 1754–1760 (2009).

394 42. H. Li *et al.*, The Sequence Alignment/Map format and SAMtools. *Bioinform*. **25**, 2078–2079
395 (2009).
396 43. Broad Institute, Picard Toolkit. *GitHub repository* (2019).
397 44. H. Li, A statistical framework for SNP calling, mutation discovery, association mapping and
398 population genetical parameter estimation from sequencing data. *Bioinform*. **27**, 2987–2993
399 (2011).
400 45. P. Danecek *et al.*, The variant call format and VCFtools. *Bioinform*. **27**, 2156–2158 (2011).
401 46. J. K. Pritchard, M. Stephens, P. Donnelly, Inference of population structure using multilocus
402 genotype data. *Genetics*. **155**, 945–959 (2000).
403 47. J. K. Pickrell, J. K. Pritchard, Inference of Population Splits and Mixtures from Genome-Wide
404 Allele Frequency Data. *PLoS Genetics*. **8**, e1002967 (2012).
405 48. P. A. Hohenlohe, S. J. Amish, J. M. Catchen, F. W. Allendorf, G. Luikart, Next-generation RAD
406 sequencing identifies thousands of SNPs for assessing hybridization between rainbow and
407 westslope cutthroat trout. *Mol. Ecol. Resour.* **11**, 117–122 (2011).
408 49. R. Gargiulo, T. Kull, M. F. Fay, Effective double-digest RAD sequencing and genotyping
409 despite large genome size. *Mol. Ecol. Resour*. **21**, 1037–1055 (2020).
410 50. T. Jombart, I. Ahmed, adegenet 1.3-1: new tools for the analysis of genome-wide SNP data.
411 *Bioinform*. **27**, 3070–3071 (2011).
412 51. N. Patterson *et al.*, Ancient Admixture in Human History. *Genetics*. **192**, 1065–1093 (2012).
413 52. D. A. Marques, K. Lucek, V. C. Sousa, L. Excoffier, O. Seehausen, Admixture between old
414 lineages facilitated contemporary ecological speciation in Lake Constance stickleback. *Nat.*
415 *Commun*. **10**, 4240 (2019).
416 53. X. Liu, Y.-X. Fu, Stairway Plot 2: demographic history inference with folded SNP frequency
417 spectra. *Genome Biol.* **21**, 280 (2020).

418 54. F. Pina-Martins, D. N. Silva, J. Fino, O. S. Paulo, Structure_threader: An improved method for
419 automation and parallelization of programs structure, fastStructure and MavericK on multicore
420 CPU systems. *Mol. Ecol. Resour*. **17**, e268–e274 (2017).
421 55. D. A. Earl, B. M. VonHoldt, STRUCTURE HARVESTER: a website and program for
422 visualizing STRUCTURE output and implementing the Evanno method. *Conserv. Genet.*
423 *Resour.* **4**, 359–361 (2012).
424 56. M. Petr, B. Vernot, J. Kelso, admixr-R package for reproducible analyses using ADMIXTOOLS.
425 *Bioinform*. **35**, 3194–3195 (2019).
426 57. R. Schwarz, U. Piatkowski, H. J. T. Hoving, Impact of environmental temperature on the
427 lifespan of octopods. *Mar. Ecol. Prog. Ser*. **605**, 151–164 (2018).
428 58. R. Schwarz, H.-J. Hoving, C. Noever, U. Piatkowski, Life histories of Antarctic incirrate
429 octopods (Cephalopoda: Octopoda). *PLoS One*. **14**, e0219694 (2019).
430 59. B. Robison, B. Seibel, J. Drazen, Deep-Sea Octopus (*Graneledone boreopacifica*) Conducts the
431 Longest-Known Egg-Brooding Period of Any Animal. *PLoS One*. **9**, e103437 (2014).
432 60. B. L. Whitelaw *et al.*, Adaptive venom evolution and toxicity in octopods is driven by extensive
433 novel gene formation, expansion, and loss. *Gigascience*. **9**, giaa120 (2020).
434 61. A. H. Patton *et al.*, Contemporary Demographic Reconstruction Methods Are Robust to Genome
435 Assembly Quality: A Case Study in Tasmanian Devils. *Mol. Biol. Evol*. **36**, 2906–2921 (2019).
436 62. R. K. Bagley, V. C. Sousa, M. L. Niemiller, C. R. Linnen, History, geography and host use shape
437 genomewide patterns of genetic variation in the redheaded pine sawfly (*Neodiprion lecontei*).
438 *Mol. Ecol*. **26**, 1022–1044 (2017).
439 63. N. Marchi, F. Schlichta, L. Excoffier, Demographic inference. *Curr. Biol.* **31**, R276–R279
440 (2021).

441 64. P. Momigliano, A. B. Florin, J. Merilä, Biases in Demographic Modeling Affect Our
442 Understanding of Recent Divergence. *Mol. Biol. Evol*. **38**, 2967–2985 (2021).
443 65. J. Choin *et al.*, Genomic insights into population history and biological adaptation in Oceania.
444 *Nature*. **592**, 583–589 (2021).
445 66. T. R. Ranallo-Benavidez, K. S. Jaron, M. C. Schatz, GenomeScope 2.0 and Smudgeplot for
446 reference-free profiling of polyploid genomes. *Nat. Commun*. **11**, 1432 (2020).
447 67. M. Kolmogorov, J. Yuan, Y. Lin, P. A. Pevzner, Assembly of long, error-prone reads using
448 repeat graphs. *Nat. Biotechnol*. **37**, 540–546 (2019).
449 68. B. J. Walker *et al.*, Pilon: An Integrated Tool for Comprehensive Microbial Variant Detection
450 and Genome Assembly Improvement. *PLoS One*. **9**, e112963 (2014).
451 69. B. Langmead, S. L. Salzberg, Fast gapped-read alignment with Bowtie 2. *Nat. Methods*. **9**, 357–
452 359 (2012).
453 70. C. A. Souza *et al.*, Efficiency of ddRAD target enriched sequencing across spiny rock lobster
454 species (Palinuridae: *Jasus*). *Sci. Rep*. **7**, 6781 (2017).
455 71. J. Catchen, P. A. Hohenlohe, S. Bassham, A. Amores, W. A. Cresko, Stacks: an analysis tool set
456 for population genomics. *Mol. Ecol.*. **22**, 3124–3140 (2013).
457 72. T. Andermann *et al.*, A Guide to Carrying Out a Phylogenomic Target Sequence Capture Project.
458 *Front. Genet.* **10**, 1407 (2020).
459 73. A. F. A. Smit, R. Hubley, P. Green, RepeatMasker Open-4.0 (2015) (available at
460 http://www.repeatmasker.org).
461 74. I. Zarrella *et al.*, The survey and reference assisted assembly of the Octopus vulgaris genome.
462 *Sci. Data.* **6**, 13 (2019).

Acknowledgments:

We thank the Australian Antarctic Division (AAD), Alfred Wegener Institute for Polar and Marine Research (AWI), British Antarctic Survey (BAS), Museum Victoria (MV), National Institute of Water and Atmospheric Research (NIWA) and George Jackson for assistance and samples for genetic analysis. We are grateful to Toni Jernfors (University of Jyväskylä) for sequencing assistance.

Funding:

Australian Research Council (ARC) Discovery grant DP190101347 (JMS, NGW, NRG, TRN)

Thomas Davies Research grant (Australian Academy of Science) (JMS)

David Pearse bequest (SCYL)

Antarctic Science Bursary (SCYL)

Antarctic PhD student support grant (Antarctic Science Foundation) (SCYL)

Australasian eResearch Organisations (AeRO) Cloud Grant (SCYL)

CoSyst grant (JMS, PCW)

Finnish Academy grant 305532 (PCW)

Australian Research Council (ARC) SRIEAS Grant SR200100005 Securing Antarctica's Environmental Future

Scientific Committee on Antarctic Research (SCAR) INSTANT programme

484 **Author contributions:**

485 Conceptualization: NGW, NRG, TRN, JMS

486 Methodology: SCYL, NGW, CNSS, JMS

487 Investigation: SCYL

488 Formal Analysis: SCYL, IRC

489 Visualization: SCYL

490 Funding acquisition: SCYL, NGW, NRG, TRN, PCW, JMS

491 Resources: PCW, ALA, FCM, KL

492 Supervision: NGW, CNSS, JMS

493 Writing – original draft: SCYL

494 Writing – review & editing: SCYL, NGW, NRG, TRN, PCW, CNSS, IRC, ALA, FCM,
495 KL, JMS

496

497 **Competing interests:**

498 Authors declare that they have no competing interests.

499

500 **Data and materials availability:**

501 The ddRADseq data of Southern Ocean octopus generated for target capture bait design is
502 deposited on National Centre for Biotechnology Information (NCBI) under the BioProject
503 PRJNA853080, with Sequence Read Archive (SRA) accessions SRR19893055–SRR19893494.
504 The target capture of ddRAD loci data in *Pareledone turqueti* is deposited under the BioProject

PRJNA853871, with SRA accessions SRR19892485–SRR19892582. The draft partial genome of *P. turqueti* is available for download from https://www.marine-omics.net/resources/. All software used for data analyses in this study is publicly available. Detailed methods including scripts and command used to perform all analyses are provided at https://github.com/sallycylau/WAIS_turqueti.

Supplementary Materials:

Materials and Methods

Supplementary Text

Figs. S1 to S10

Tables S1 to S5

Data S1 to S2

References (*36–74*)